Hydrophobization of paper intended for packaging

D. Dergham[a], M. Ouchabane[a], S. Hadjira[b], F. Lekoui[a], and S. Hassani[a]
[a]*Centre de Développement des Technologies Avancées Cité du 20 Août 1956, Baba Hassan, Alger, Algérie.*
e-mail: ddergham1@gmail.com
[b]*Département de Génie des Procédés, Université Saad Dahleb, Blida, Algérie*

Received 18 October 2021; accepted 17 November 2021

The proposed manuscript deals with packaging surface paper treatment with plasma enhanced chemical vapor deposition (PECVD) technique. To do this, paper samples were held on a grounded substrate to be in contact with methane(CH_4) plasma created by the upper cathode to grow hydrogenated carbon films ($a - C : H$) on top surface of paper. The treatment duration was maintained for 5, 10, 15 and 20 min while pressure and power have been kept constant at 8×10^{-2} and 100 W, respectively. After deposition the surface sample has undergone structural and morphological characterization by Scanning Electron Microscopy (SEM), Atomic Force Microscopy (AFM) and Fourier Transform Infrared Spectroscopy (FTIR) is performed to reveal the bonding structure. The surface wettability of the treated samples was evaluated by contact angle (CA) measurement. The results of CA show the change of surface paper from hydrophilic to hydrophobic and even superhydrophobic with a maximum contact angle equal 156°.

Keywords: Hydrophobic surface; a-C:H layers; PECVD; paper substrates.

DOI: https://doi.org/10.31349/RevMexFis.68.031006

1. Introduction

The fascinating water repellents of many biological surfaces, in particular, plant leaves such as Lotus leaf, in the feathers of birds, such as peacock, and also in cuticle of insects, whose self-cleaning surface has a contact angle approaching 180° inspire us to imitate such functionality in numerous industrial applications. Indeed, such properties are ensured by the presence of a special structure and morphology, [1,2] or by the presence of a thin layer of material by deposition or etching [3,4] that provides the desired functionality. As with the lotus leaf, the rose petal has a hydrophobic wax layer, Dragonflies, with a very thin stable and super-hydrophobic wings and self-cleaning has recently attracted great interest for fundamental research as well as practical applications, such as self-cleaning, impermeability, anti-icing [5-7], waterproof clothes, corrosion prevention, anti-fouling, microelectronics, and biomedical applications [8-12]. The first attempt to understand the relationship between wettability and roughness dates back to (1936) Wenzel [13], he noted that the hydrophobic character of a material is improved by the presence of a special surface textures. He attributed this behavior to the increase in the effective surface, because the liquid perfectly matches the contours of the roughness. The morphology of the coating surface can be modified and the hydrophobic properties can be improved by the introduction of several materials such as silicone, titanium oxide and other materials [14-16]. To obtain micro-structured surfaces several methods can be used [17] including etching, vapor deposition, phase separation, nanoparticle filling, etc... To modify surface morphology, Hsieh [17] introduced TiO_2 nanoparticles in a perfluoroalkyl methacrylate copolymer to produce a rough surface. Thies *et al.* [18] added activated SiO_2 nanoparticles (with a diameter of (10-15 nm) to methyltrimethoxy silane $CH_3Si(OCH_3)_3$, and obtained coatings with good hydrophobic and mechanical properties. In this article, we have prepared different surface microstructures by surface treatment using CH_4 plasma; the effect of treatment time as well as surface morphology and microstructure on surface hydrophobicity have been investigated.

2. Experimental setup

In this work thin hydrogenated carbon $(a - C : H)$ layers were deposited on the 20×20 mm paper substrate by PECVD technique., The discharge was ignited by RF(13.56 MHz) power. After the introduction of the substrates, an Ar plasma cleaning operation was followed for 5 min at a gas pressure of 2×10^{-2} mbar and a V_{dc} bias of 450 V in order to remove any contaminants on the surface and to activate the surface, and then the methane gas was introduced into the reaction chamber. The main part of the experimental installation is illustrated in Fig. 1 (a,b) and details can be found elsewhere in Refs. [19,20]. It consists of an electrode system made up of flat 10 cm diameter parallel discs, the distance between electrodes is 12 cm, the hollow upper electrode is connected to the RF generator (13.56 MHz) and the lower electrode is grounded once. The gas flow has been changed via the mass flow controller and maintained at 8×10^{-2} mbar inside the chamber deposition, while the deposition time is varied be-

TABLE I. Experimental parameters of surface paper treatment.

Sample	E1	E2	E3	E4
Time (min)	5	10	15	20
Pressure (mbar)	8×10^{-2}	8×10^{-2}	8×10^{-2}	8×10^{-2}
Power (W)	100	100	100	100
Bias Voltage, V_{dc} (V)	170	170	170	170

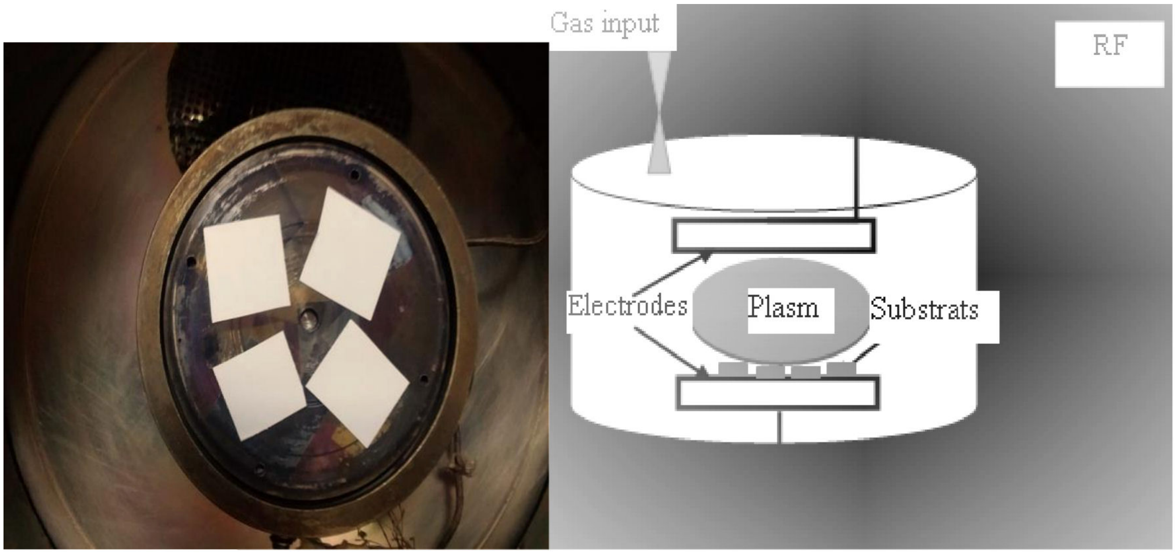

FIGURE 1. a) Substrates used for deposits. b) Scheme of a PECVD reactor chamber used for deposition.

tween 5 min, 10, 15 and 20 min. The input power was maintained at constant value of 100 W and a self-bias voltage (V_{dc}) of 170 V at the upper electrode. The experimental parameters are summarized in Table I.

In order to investigate the film's characteristic, the surface morphology of the as deposited thin films was analyzed by means of scanning electron microscope (SEM, JEOLJSM-6360LV) while surface topography and roughness of the films were evaluated by AFM in contact mode by a Nanosurf Flex-AFM system equipped with a 10×10 μm high-resolution scanner. AFM images were recorded with a resolution of 256×256 pixels over scanning areas of 2×2 μm, and the Gwyddion software was used for image processing and surface roughness calculations [21]. To characterize the bonding structure of the deposited films an FTIR (Bruker, EQUTNOX 55 model) spectrophotometer with wavenumber range of $400 - 4000$ cm^{-1} was employed. The water contact angles of the films measurements were determined by GBX "$Digidrop$" optical contact angle measurer instrument.

3. Results and discussion

3.1. SEM image of untreated paper

The micrographs obtained by scanning electron microscopy (SEM) of the untreated paper sheets are shown in Fig. 2. Surface micrographs show a homogeneous and relatively regular coating, with cellulose fibers which fills the pores appear on the surface. It should be noted that the surface display single fibers which constitutes the matrix of the organic material. These fibers are arranged in an unordered manner and appear structured like those of polymeric materials. The white parts in the figure are supposed to be lignin that goes into paper making.

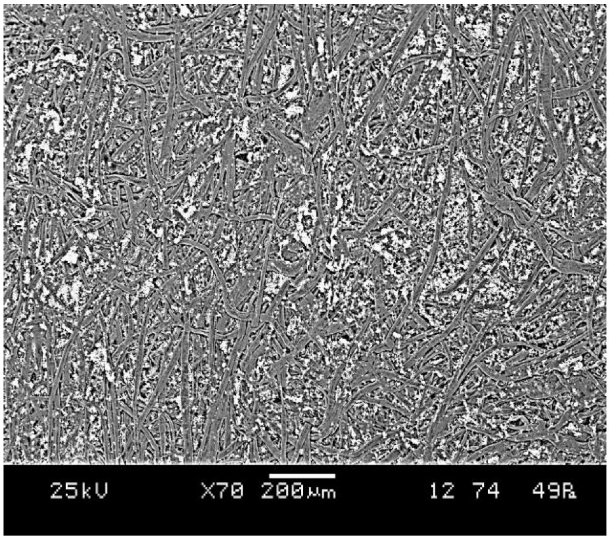

FIGURE 2. SEM image: paper sample without treatment.

3.2. Roughness measurement

To measure the roughness of the treated surfaces, atomic force microscopy (AFM) analysis was performed on paper samples treated with CH_4 plasma at different time. As known, surface roughness is most often described by amplitude parameters, such as mean square deviation, and standard deviation. To analyze and compare the surface roughness of the deposited thin films for each surface treatment we measured the roughness in particular; the root mean square (RMS) as depicted by Fig. 3. The registered values are summarized in the Table II and illustrated by Fig. 3 in 2D and 3D images. As can be seen from Table II, surface roughness decreases from 1.64 to 0.97 nm, and then increases to 1.66 nm and 1.7 for more deposition time. This variation of RMS

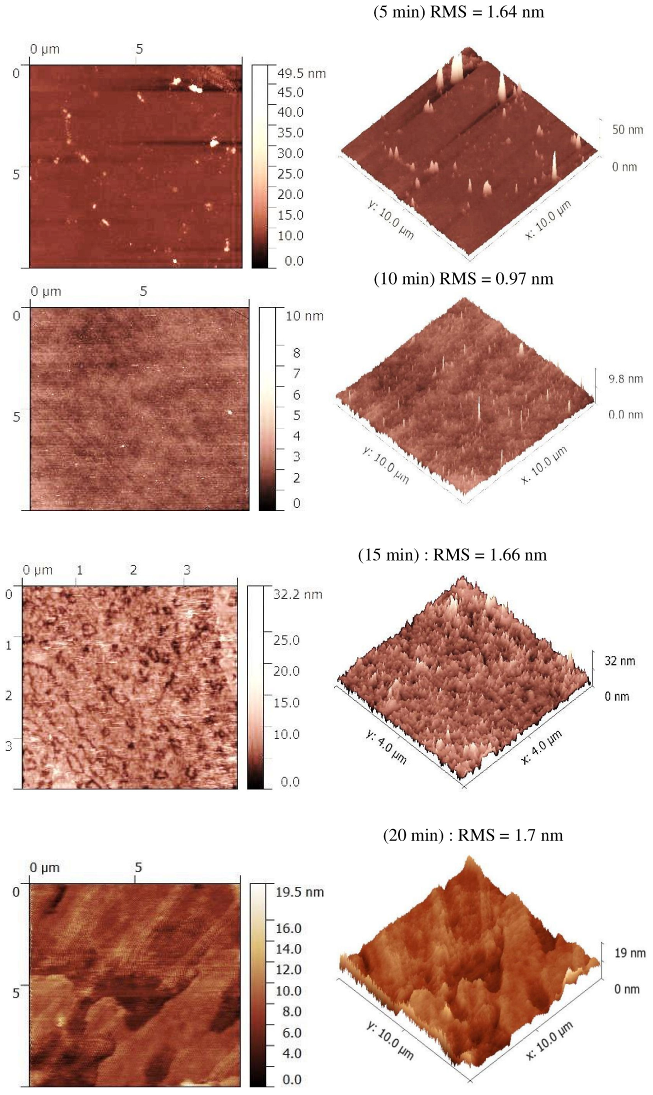

FIGURE 3. AFM 2D and 3D images.

TABLE II. Surface roughness of the films.

Sample	Time (min)	Roughness (nm)	Contact angle (°)
E1	5	1.64	153.8
E2	10	0.97	137.7
E3	15	1.66	149.2
E4	20	1.7	156

can be explained by; initially, the surface paper is more rough and as we start the treatment the surface texture is modified by filling up irregularities and pockets resulting in roughness decreasing giving up to a value of 1.64 nm. By continuing the deposit, these pockets and irregularities become more filled to give rise a smooth surface with 0.97 nm of roughness with almost total disappearance of irregularities as shown in Fig. 3. However, surprisingly as the growth process continues for longer time the roughness does not continue to take low values but increases towards 1.66 nm and 1.7 nm with the reappearance of a uniform texture on top surface paper. This means that the top surface paper is covered by a thin layer of hydrogenated carbon film that is consisted by a mixture of sp^2 and sp^3 carbon hybridization. Some authors [21-23] in their studies attributed the increase of surface roughness to the increase in growth of sp^2 carbon bonds and the increase in clusters size, and vice versa. On the other hand, Pandey *et al.* [24] reported that the higher the sp^3 fraction is, the smoother is the surface. K. N. Pandiyaraj *et al.* [25] have attributed the difference in RMS with sp^3 fraction by changing the values of bias potential of the substrate holder, which is not the case in our experiments surface treatment. Consequently, the sp^3 fraction in our thin films does not change since the substrate holder is grounded for all treatments. However, the sp^2 fraction in DLC films can change with film thickness as reported by Scharf and Singer [26] in their study of diamond-like carbon films by Raman spectroscopy. This finding leads us to suppose that the increase in roughness can be attributed to the clustering of sp^2 bonds as mentioned before.

3.3. Contact angle measurement

The effect of CH4 plasma on the wettability was investigated by measuring the contact angle of the sessile water droplet on the paper surface. Figure 4 presents the images of the water contact angle variation as a function of deposition time. One can observe that all the coating surfaces have become super-hydrophobic, except the coating deposited for 10 min which is exhibiting a hydrophobic behavior. In Fig. 5, the variation of the contact angle and roughness versus deposition time is illustrated; the samples treated for 5 min exhibits a hydrophobic character with a contact angle equal 153.8° and Rrms equal to 1.64 nm. Increasing the time treatment to 10 min the Rrms decrease to the 0.97 nm, consequently the contact angle decreases to 137.7°, then Rrms increase to 1.66 nm and 1.7 nm for a treatment at 15 min and 20 min

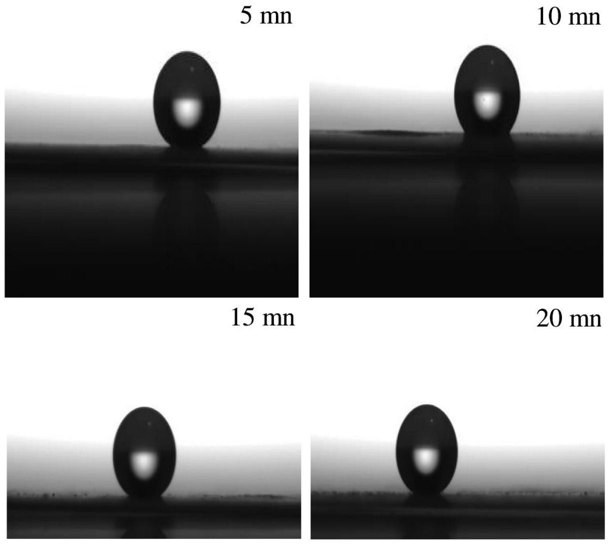

FIGURE 4. Water drop images for contact angle measurement.

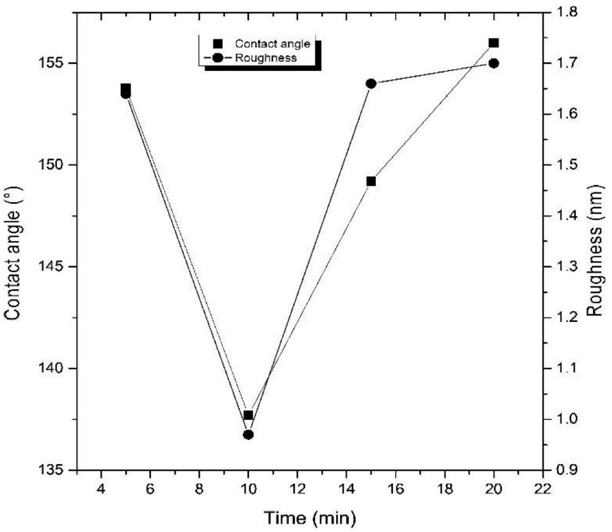

FIGURE 5. Contact angle and roughness vs deposition time.

respectively, which leads to an increase in the contact angle to 149.2° and 156°, respectively. Generally, hydrophobicity and hydrophilicity of surfaces are influenced by surface roughness, and surface energy, a rough surface and a low surface energy gives a superhydrophobic surface [27] the surface energy [28] includes two important components, dispersion and polar components. Polar components represent the surface interactions, which are related to dipoles, while dispersive component represents the surface interactions, which are based on temporary variation in the electron density. Bhushan and Jung [29] reported that two main requirements for a super-hydrophobic surface are that the surface should be rough and has a low surface energy with a special focus on roughness which is usually a more critical property than the low surface energy. Such assumption is confirmed by Fig. 5 where contact angle and roughness are plotted together as a function of deposition time. At first glance, one can conclude that CA and RMS exhibit a same behavior and there will be a relationship between the two parameters as reported above. On one side, the roughness of the surface serve to trap enough air, which prevents the water drops from being in perfect contact with the surface, which facilitates the sliding of the water drops. On the other side, the presence of CH_x radicals has an important influence on the surface hydrophobicity. N. Sooryun *et al*. [30], indicate that the alkane group has an intrinsic critical surface tension, the contact angle can show a certain value if the whole surface is covered by the functional group layer such as C−H stretch, CH_2 bend and CH_3 bend, which proves the hydrophobicity formation by the plasmas.

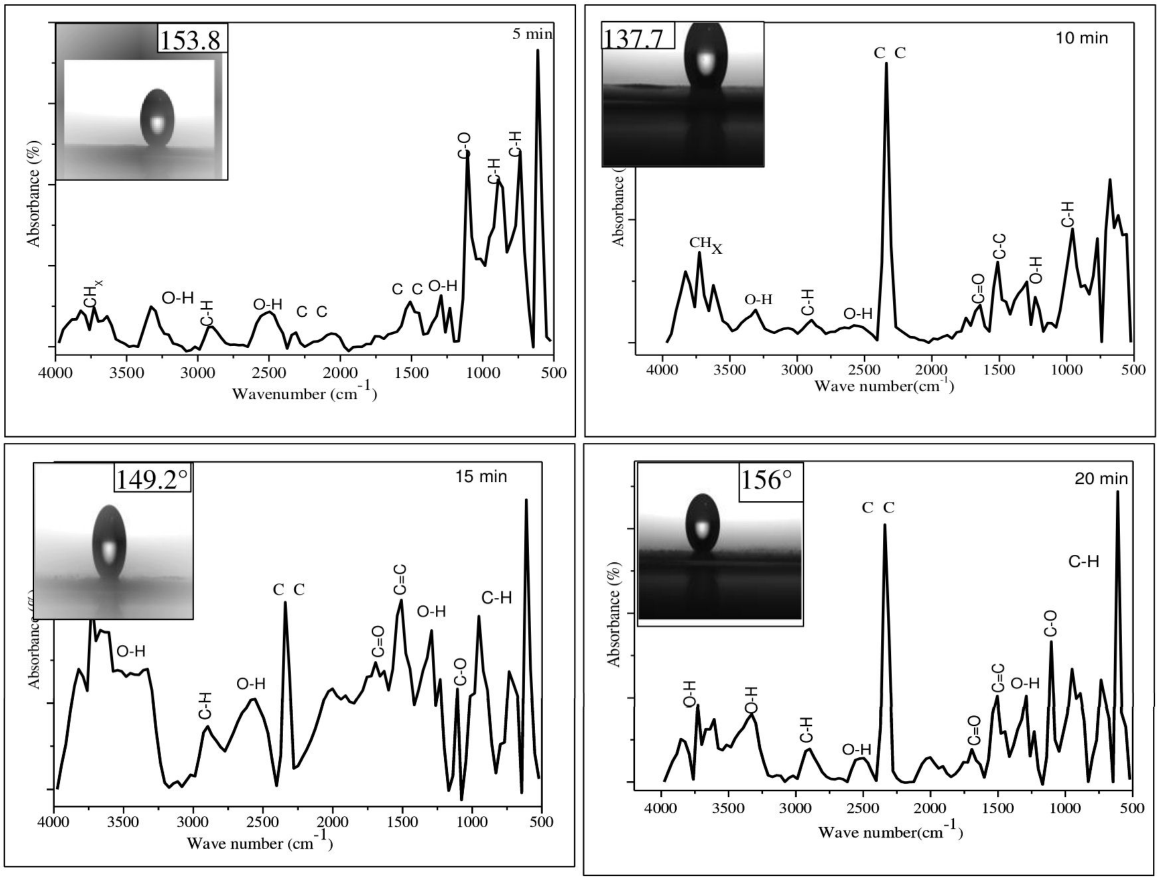

FIGURE 6. FTIR Spectra of hydrogenated carbon thin films.

3.4. FTIR Studies of chemical bands

Now let us determine the presence of functional groups on the surface of the treated paper by using FTIR analysis. Figure 6 shows the FTIR spectra of all treated surface paper. As one can see for all samples, an absorption band occurs between 737 and 613 cm^{-1}. This bond is decomposed into three strong peaks assigned to C$-$H out of plane vibrations. A strong peak appears at 1104 cm^{-1} for samples deposited at 5 min, and then disappears for samples deposited at 10 min. The same peak appears again shifted towards the weaker frequencies for samples deposited at 15 min and 20 min. This peak is attributed to the stretching vibration of C$-$O as reported by N. V. Farinella Van. P. D. *et al.* [31] who found a peak at 1110 cm^{-1} of C$-$O in the lignin structure. Also, the absorption peak appearing at 1293 cm^{-1} is assigned to stretching bands in C$-$O [32], which shifts towards high frequencies for samples treated during 20 mn. The band at 1512 is attributed to C$=$C aromatic stretching modes [33] while at appearing at 2917 cm^{-1} is assigned to antisymmetric stretching $sp_3$$-C-H_n$ as confirmed by some other authors [23,34,35]. A weak peak is observed at 2324 cm^{-1} attributed to the C$-$C bends, and becomes strong with deposition time. Such variation in the relative intensity suggests a removal and incorporation of species *i.e.* groups are reincorporated in the same proportion as they are removed. The peaks at 3325 cm^{-1}, 3330 cm^{-1} and 3732 cm^{-1} corresponds to O$-$H stretching bands [36,37] and the peak at 3732 cm^{-1} are assigned to O$-$H stretching while the same peak around $3600 - 3800$ cm^{-1} is identified by [38] and attributed to an isolated -OH stretching vibration. All CH$_x$ molecules are the result of methane molecule (CH$_4$) dissociation, giving rise to radicals such as CH$_3$, CH$_2$, C$_2$H$_5$, C$_2$H$_6$ etc. while the oxygen entering in the OH bond formation comes from the residual vacuum generally equal to 2×10^{-5} mbar. The presence of functional groups (non-polar such as CH$_x$) will prevent the entry of water molecules in the polar bonds in most of the surface of the paper, thus contributing to the improvement of the hydrophobic properties of the surface of the glass [39], thus contributing to the improvement of the hydrophobic properties of the paper surface.

4. Conclusion

The study we carried out concerns the treatment of paper surface plasma enhanced chemical vapor deposition (PECVD) technique by using CH_4 gas. Paper samples in contact with the plasma leads to the deposition of a thin layer of hydrogenated carbon, the thickness of which was varied with the deposition time while other experimental parameters were kept constant during all manipulations. In summary, the presented results on hydrophobicity of surface paper have been discussed according to AFM, contact angle and FTIR measurements. The concluding remarks that can be drawn are as follows:

- After a contact with CH$_4$ plasma in a PECVD reactor a thin layer of hydrogenated carbon material is deposited,
- Surface paper roughness is in the order of approximately 1 nm to 1.7 nm after a surface treatment ranging from 5 min to 20 min.
- The deposition of a thin layer of hydrogenated carbon on surface paper gives hydrophobicity and even superhydrophobicity to its surface,
- The FTIR spectroscopy confirms the presence of nonpolar groups on the surface that enhance hydrophobicity,
- The presented results confirm the existence of a relationship between hydrophobicity and roughness promoted by a clustering of sp^2 hybridization with film thickness,

In conclusion, the encouraging results promise the efficient application of hydrogenated carbon to surface paper modification, thus protecting and giving it a long life with minimal damage upon contact with water.

---

1. L. B. Boinovich and A. M. Emelyanenko, principles of design, properties and applications, Hydrophobic materials and coatings: *Russian Chemical Reviews*, **77** (2008) 583.
2. S. Pieter, Wetting and hydrophobic modification of cellulose surfaces for paper applications. *Journal of Materials Science* **48** (2013) 6455.
3. L. Xie, Z. Tang, L. Jiang, V. Breedveld and D. W. Hess. Creation of superhydrophobic wood surfaces by plasma etching and thin-film deposition, *Surface and coatings technology*, **281** (2015) 125.
4. X. Liu and C. Luo. Fabrication of super-hydrophobic channels, *Journal of Micromechanics and Microengineering*, **20** (2010) `https://doi.org/10.1088/0960-1317/20/2/025029`.
5. W. Barthlott, and C. Neinhuis, Purity of the sacred lotus, or escape from contamination in biological surfaces, *Planta*, **202** (1997) 1.
6. C. Neinhuis and W. Barthlott, Characterization and distribution of water-repellent, self-cleaning plant surfaces, *Annals of botany*, **79** (1997) 667.
7. Otten, Alexander, Herminghaus and Stephan. How plants keep dry: a physicist's point of view, *Langmuir*, *20* (2004) 2405.

8. T. A. Desai, D. J. Hansford, L. Leoni, M. Essenpreis and M. Ferrari, Nanoporous anti-fouling silicon membranes for biosensor applications, *Biosensors and Bioelectronics*, **15** (2000) 453.
9. B. Jeong and A. Gutowska, Lessons from nature: stimuli-responsive polymers and their biomedical applications, *Trends in biotechnology* **20** (2002) 305.
10. M. Liu, Y. Lu, J. Zhang, S. Xia and J. Yang, MEMS/microelectronics self-assembly based on analogy of Langmuir-Blodgett approach, *Microelectronic Engineering*, **86** (2009) 2279.
11. T. Liu, Y. Yin, S. Chen, X. Chang, and S. Cheng, Superhydrophobic surfaces improve corrosion resistance of copper in seawater, *Electrochimica Acta*, *52* (2007) 3709.
12. Q. B. Meng, S-II. Lee, C. Nah and Y-S. Lee, Preparation of waterborne polyurethanes using an amphiphilic diol for breathable waterproof textile coatings, *Progress in Organic Coatings*, **66** (2009) 382.
13. R. N. Wenzel, Resistance of solid surfaces to wetting by water, *Industrial & Engineering Chemistry* **28** (1936) 988.
14. G. R. J. Artus, S. Jung, J. Zemmermann and H.-P. Gautschi, Silicone nanofilaments and their application as superhydrophobic coatings, *Advanced Materials*, **18** (2006) 2758.
15. N. Zhao *et al*., Fabrication of biomimetic superhydrophobic coating with a micro-nano-binary structure, *Macromolecular rapid communications*, **26** (2005) 1075.
16. L. Huang, K. Chen, C. Len and R. Yang, Fabrication and characterization of superhydrophobic high opacity paper with titanium dioxide nanoparticles, *Journal of Materials Science*, **46** (2011) 2600.
17. C.-T. Hsieh, J. M. Chen, R.-R. Kuo and T.-S. Lin, Influence of surface roughness on water-and oil-repellent surfaces coated with nanoparticles, *Applied Surface Science*, **240** (2005) 318.
18. J. C. Thies, G. J. W. Meijers, J. A. Pitkin, E. E. Currie, C. F. Tronche and JE.Southwell, Hydrophobic coatings comprising reactive nano-particles , Patent Application Publication (2006) US 2006/0286305 A1.
19. M. Ouchabane, M. Aoucher, A. Sekkal, K. Henda and H. Lahmar, Structural Analysis of Diamond-Like Carbon Films Deposited by RF (13.56 MHz) in a Methane Gas Plasma Atmosphere, Plasma Processes and Polymers (2005) 87, https://doi.org/10.1002/3527605584.ch7.
20. S. Djerourou, M. Djebli, and M. Ouchabane, Plasma parameters of RF capacitively coupled discharge: comparative study between a plane cathode and a large hole dimensions multi-hollow cathode, *The European Physical Journal Applied Physics* **85** (2019) 10801.
21. D. Neas, and P. Klapetek, Gwyddion-Free SPM (AFM, SNOM/NSOM, STM, MFM,...) data analysis software.
22. Z. Tang, Z. J. Zhang, K. Narumi, Y. Xu, H. Naramoto and S. Nagai, Effect of mass-selected ion species on structure and properties of diamond-like carbon films, *Journal of applied physics* **89** (2001) 1959.
23. S. Kataria, S. Dhara, H. C. Barshilia, S. Dash, and A. K. Tyagi, Evolution of coefficient of friction with deposition temperature in diamond like carbon thin films, *Journal of applied physics*, **112** (2012) 023525.
24. M. Pandey, D. Bhatacharyya, D. S. Patil, K. Ramachandran and N. Venkatramani, Diamond-like carbon coatings: AFM and ellipsometric studies, *Surface and coatings technology*, **182** (2004) 24.
25. K. N. Pandiyaraj *et al.*, Influence of bias voltage on diamond like carbon (DLC) film deposited on polyethylene terephthalate (PET)film surfaces using PECVD and its blood compatibility, *Diamond and Related Materials* **19** (2010) 1085.
26. T. W. Scharf and I. L. Singer, Thickness of diamond-like carbon coatings quantified with Raman spectroscopy, *Thin Solid Films* **440** (2003) 138.
27. S.-M. Baek, T. Shirafuji, S.-P. Cho, N. Saito and O. Takai, Oxygen Gas Barrier Properties of Hydrogenated Amorphous Carbon Thin Films Deposited with a Pulse-Biased Inductively Coupled Plasma Chemical Vapor Deposition Method, *Japanese Journal of Applied Physics*, **49** (2010) 08JF10.
28. W. Xie *et al.*, Colorful Carbon Nanopopcorns Formed by Codepositing C60 with Diamond-like Carbon Followed by Reaction with Water Vapor, *Chemistry Letters*, **44** (2015) 1205.
29. B. Bhushan and Y. C. Jung, Natural and biomimetic artificial surfaces for superhydrophobicity, self-cleaning, low adhesion, and drag reduc, *Progress in Materials Science*, **56** (2011) 1.
30. S. Noh, and S. Youn Moon, Formation and characterization of hydrophobic glass surface treated by atmospheric pressure He/CH4, *Journal of applied physics*, **115** (2014) 043307.
31. N. Farinella, G. Matos and M. Arruda, Grape bagasse as a potential biosorbent of metals in effluent treatments, *Bioresource technology*, **98** (2007) 1940.
32. M. Zhou and L. Andrews, Infrared spectra of the C2O4+ cation and C2O4+ anion isolated in solid neon, *The Journal of Chemical Physics*, **110** (1999) 6820.
33. V.-P. Dinh, T.-D.-T. Huynh, H.M.Le and D.N.Van, Insight into the adsorption mechanisms of methylene blue and chromium (III) from aqueous solution onto pomelo fruit peel, *RSC advances*, **9** (2019) 25847.
34. M. Roy, K. Mali, N. Joshi and D. Misra, Deposition of hydrogenated amorphous carbon films with enhanced sp3-C bonding on nanocrystalline palladium interlayer, *Diamond and Related Materials*, **16** (2007) 517.
35. V. P. Tolstoy, I. V. Chernyshova and V. A. Skryshevsky, Handbook of infrared spectroscopy of ultrathin films 2003: John Wiley & Sons.
36. E. Mohsen Soltani, Z. Ghorannevis and M. Shirazi, Effect of Ar/CH$_4$ mixture ratio on properties of Ag/C: H nanocomposite prepared by DC sputtering, *Advances in Materials Science and Engineering* (2013) https://dx.doi.org/10.1155/2013/142450.
37. D. Banerjee, D. Sen, and K. Chattopadhyay, Simple chemical synthesis of porous carbon spheres and its improved field emission by water vapor adsorption, *Microporous and mesoporous materials*, **171** (2013) 201.
38. R. Paul *et al.*, Synthesis and characterization of composite films of silver nanoparticles embedded in DLC matrix prepared by plasma CVD technique, *The European Physical Journal-Applied Physics* **47** (2009), https://doi.org/10.1051/epjap/2009086.
39. Y. Kurahashi, H. Tanaka, M. Terayama and J. Sugimura, Effects of environmental gas and trace water on the friction of DLC sliding with metals, *Micromachines*, **8** (2017) 217, https://doi.org/10.3390/mi8070217.